Article
Chinese Science Bulletin
Optics
May 2012 Vol.57 No.14: 1648–1654
doi: 10.1007/s11434-012-5057-7

Phase-error restraint with the empirical mode decomposition method in phase measurement profilometry

WEN YongFu, CHENG HaoBo*, GAO Ya & ZHANG HuiJing

School of Optoelectronics, Beijing Institute of Technology, Beijing 100081, China

Received October 11, 2011; accepted December 13, 2011

Phase measurement profilometry (PMP) uses a digital projector and a camera for 3D shape measurement. However, the nonlinear response of the measurement system causes the captured perfect sinusoidal fringe patterns to become non-sinusoidal waveforms, which results in phase and measurement errors. We perform a theoretical analysis of the phase error resulting from non-sinusoidal fringe patterns. Based on a derived phase-error expression, the empirical mode decomposition (EMD) method is introduced to restrain nonlinear phase error and improve the precision in evaluating the phase distribution. A computer simulation and experimental results prove that the proposed method can eliminate possible phase-error in PMP.

phase measurement profilometry, empirical mode decomposition, phase error, fringe analysis

Citation: Wen Y F, Cheng H B, Gao Y, et al. Phase-error restraint with the empirical mode decomposition method in phase measurement profilometry. Chin Sci Bull, 2012, 57: 1648–1654, doi: 10.1007/s11434-012-5057-7

In recent years, digital fringe projection techniques have received considerable attention for noncontact 3D shape measurement, such as in Moiré topography, Phase Measurement Profilometry (PMP) and Fourier Transform Profilometry (FTP). In PMP [1], the phase mapping from digitized N frames fringe data to wrapping phase is a point-to-point operation. The reflective ratio and background have little influence on phase calculations. Thus, PMP has become an important 3-D measurement method.

The main technique of PMP is to extract the phase from the captured fringe patterns. The drawback of a PMP system is that it is sensitive to the nonlinear elements of the measurement system such as the detector nonlinearities and the nonlinear γ of the projector [2]. The ideal sinusoidal fringe patterns deform to become non-sinusoidal and introduce phase errors because of the nonlinear effect on the system. Phase-error analysis and compensation for non-sinusoidal waveforms in phase shifting profilometry have been studied [3–5]. Ref. [6] analyzes the error sources in phase-measuring interferometry. Some investigators have proposed an algorithm to compensate for the nonlinear effect of the projector–camera system for range image acquisition of objects with non-uniform albedo [7]. However, the whole calibration procedure is time consuming and laborious. Recently, much research effort has focused on developing simpler techniques to mitigate the error. Based on the derived theoretical model, the simple iterative phase compensation algorithm [8] and the cubic spline smoothing method [9] have been proposed to reduce the nonlinear phase error.

In this study, we perform theoretical analysis of the phase error resulting from the nonlinear response of the measurement system. Based on the derived phase-error expression, the empirical mode decomposition (EMD) method [10,11] is introduced to reduce nonlinear phase error and improve the precision in evaluations of phase distribution.

1 Fundamental principles

1.1 Phase-error analysis

In PMP, a digital projector is used to generate a sinusoidal fringe pattern which is projected onto the surface of the test

*Corresponding author (email: chenghaobo@tsinghua.org.cn)

object. The N frames of deformed images of the surface of the object are then modulated by the fringe patterns, which are obtained using a CCD camera. We recover the phase distribution by dealing with the deformed fringes.

The nth fringe of a sequence of N ideal deformed sinusoidal fringe images can be expressed as follows:

$$I_n(x,y) = a(x,y) + b(x,y)\cos[\varphi(x,y) + 2\pi n / N], \quad (1)$$

where, $a(x,y)$ is the background intensity, $b(x,y)$ is the intensity modulation, and $\varphi(x,y)$ is the desired phase information. Upon translation of the original grating by a fraction $1/N$ of its period, the phase of the fringe patterns by eq. (1) is shifted by $2\pi / N$ (N=3, 4, 5,…). The ideal phase can then be shown as follows [12],

$$\varphi(x,y) = \tan^{-1}\left\{\frac{\sum_{n=1}^{N} I_n(x,y)\sin[2\pi n / N]}{\sum_{n=1}^{N} I_n(x,y)\cos[2\pi n / N]}\right\}. \quad (2)$$

In the actual measurement, because of the nonlinear error of the measurement system (which includes a projector and a camera), the relationship between the input and output signal is no longer linear as shown in Figure 1. In this case, the nonlinear response of the system causes the captured perfect sinusoidal fringe patterns to become non-sinusoidal waveforms, which results in phase fluctuation errors. Therefore, the actual phase can be written as the sum of the ideal phase and the phase error caused by the measurement system. We can then obtain

$$\varphi'(x,y) = \varphi(x,y) + \Delta\varphi(x,y). \quad (3)$$

In most cases, the largest distortions affecting the measurement are probably due to the third-order nonlinearity errors. However, we should consider higher-order nonlinearity errors of the system in high-precision measurement. Then, using a universal nonlinear function, which is caused by the overall nonlinearity of the PMP system, to depict the system response function, as shown in eq. (4).

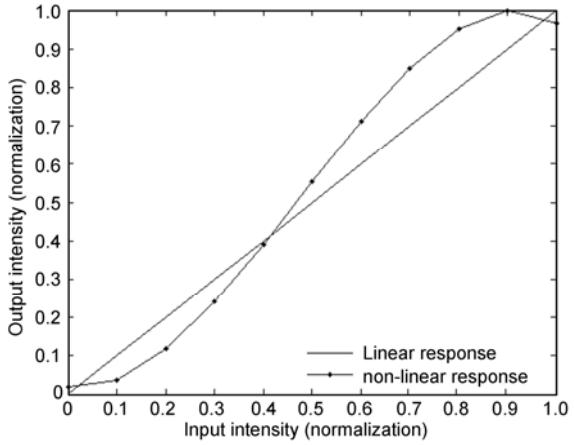

Figure 1 System intensity response function.

$$I_n^*(x,y) = \sum_{k=0}^{+\infty} \delta_k I_n^k(x,y), \quad (4)$$

where, δ and k express the response coefficient of thesystem and its orders. Therefore, by combining eqs. (1) and (4), the intensity error of the actual fringe images can be expressed as follows:

$$\mathrm{d}I_n(x,y) = I_n^*(x,y) - I_n(x,y). \quad (5)$$

To obtain the phase error, we calculate the intensity differential coefficient of eq. (2). Thus, the phase error can be expressed as follows:

$$\begin{aligned}\mathrm{d}\varphi \approx \Delta\varphi = -\Bigg\{&\sum_{n=1}^{N} I_n \cos(2\pi / N)\sum_{n=1}^{N}\mathrm{d}I_n \sin(2\pi / N) \\ &-\sum_{n=1}^{N} I_n \sin(2\pi / N)\sum_{n=1}^{N}\mathrm{d}I_n \cos(2\pi / N)\Bigg\} \\ &\Big/\Big\{[\sum_{n=1}^{+\infty} I_n \cos(2\pi / N)]^2 + [\sum_{n=1}^{+\infty} I_n \sin(2\pi / N)]^2\Big\}, \quad (6)\end{aligned}$$

$$\begin{aligned}\Delta\varphi(x,y) = -2\Bigg\{&\cos\varphi(x,y)\sum_{n=1}^{N}\mathrm{d}I_n \sin(2\pi / N) \\ &+\sin\varphi(x,y)\sum_{n=1}^{N}\mathrm{d}I_n \cos(2\pi / N)\Bigg\} \\ &\Big/\{N\cdot b(x,y)\}. \quad (7)\end{aligned}$$

By joining the eqs. (1) — (6), we obtain the phase error caused by the nonlinearity of the measurement system as in eq. (7). Thus, eq. (7) shows that the phase error is modulated by the system nonlinearity error. In the ideal state, the system response curve is a linear function and the intensity error $\mathrm{d}I_n(x,y) = 0$. Then, according to eq. (7), we know the phase error $\Delta\varphi(x,y) = 0$. However, this situation is impossible in an actual measurement.

1.2 The calculation of the theoreticals

Eq. (7) describes the phase error as a nonlinear error. To reduce the impact of the nonlinear error, we adopt a new nonlinear technique, which is called the empirical mode decomposition (EMD) method in this paper. The objective of the EMD method is to separate a nonlinear signal empirically into a set of functions which include the Intrinsic Mode Functions (IMFs) and the residual. The first IMF contains the highest frequency component of a signal while the latter contain the lower frequency components.

The procedure for extracting the IMF is referred to as a sifting process. For a given temporal signal $I(t)$, the sifting algorithm can be summarized as follows:

Step 1: The sifting process begins by identifying all local extrema in $I(t)$. The extreme maxima are then connected using the cubic splines to form the upper envelope $I_{\max}(t)$.

Similarly, the local extreme minima produce the lower envelope $I_{\min}(t)$.

Step 2: The mean of the two envelopes and an instantaneous signal can be obtained using eqs. (8), (9), respectively.

$$m(t)=\frac{I_{\max}(t)-I_{\min}(t)}{2}, \tag{8}$$

$$D(t)=I(t)-m(t). \tag{9}$$

This procedure is iterated until $D(t)$ can be considered to have a zero mean difference. Once it is obtained, $D(t)$ will become the first IMF $c_1(t)$.

Step 3: The residue is determined from the equation

$$r_1(t)=I(t)-c_1(t). \tag{10}$$

Using the residue $r_1(t)$ as a new original signal, the next IMF is gained by repeating Steps 1 and 2. Finally, the process is stopped when the residue becomes a constant or monotonic function for which IMF can no longer be decomposed. Finally, the EMD method expresses the signal data as follows:

$$I(t)=\sum_{n=1}^{m}c_n(t)+r_m(t), \tag{11}$$

where $I(t)$ is the original signal, $c_n(t)$ are the IMFs, $r_m(t)$ is a residual, and m is the total number of IMFs. The EMD method is described in detail in [7,8]. Here, we only introduce the process of the 1-D data, since this principle is easily expanded to 2-D data.

In this paper, we use the EMD method to decompose the phase into a finite number of IMFs that vary from high-frequency to low-frequency components. Because the high-order phase errors represent the high frequency components of the phase, we can subtract the decomposed high frequency components directly from the original deformed phase. We can then minimize the influence of the nonlinear response of the measurement system on the phase calculation process.

2 Computer simulation and experiments

To demonstrate the validity of the phase reduction method using EMD in Phase Measurement Profilometry, a computer simulation and experiments are carried out. In this paper, we focus on the five-step phase-shifting method. However, the method can be applied to either three- or four-step phase-shifting methods.

We carried out a computer simulation using the MATLAB software. The fundamental frequency of the simulated fringe pattern is f_0=1/16 pixel, and the size of the simulated image is 256×256 pixels. Because of the improving quality of electronic products, in most cases, the nonlinear errors of projectors and cameras are less than fifth-order. Therefore, to describe the actual measurement system better, we assume that the measurement system has fifth-order nonlinear errors. When the sinusoidal fringe images pass through this system, the fringe intensity can be expressed as follows:

$$I^*(x,y)=-0.5I^5+1.1I^4-2.2.5I^3\ I^3 +2.26I^2-0.11I+0.01. \tag{12}$$

The camera captured the reference fringe pattern and its 128th row as shown in Figure 2(a) and (b), respectively. In this figure, since combining with the fifth-order nonlinear error, the fringe pattern becomes a non-sinusoidal curve. This will cause fluctuation errors in the actual calculated phase distribution. The simulated object is a free-form model (peaks function). Figure 3(a) shows the phase distribution. The projector projected five phase-shifted fringe images and the camera captured the deformed fringe images. Figure 3(b) shows one of the deformed fringe images.

According to the eq. (2), we obtain the wrapping phase of the tested object by conventional five-step phase-shifting. We then use the phase-unwrapping algorithm and subtract the reference phase to obtain the actual phase $\varphi'(x,y)$, which is shown in Figure 4(a). Figure 4(a) shows there are

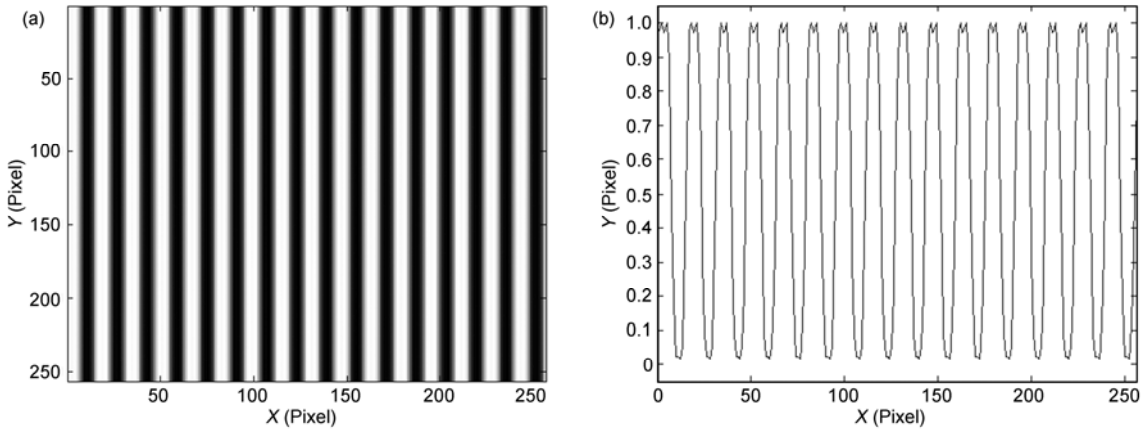

Figure 2 Fringe intensity distribution. (a) The reference fringe intensity distribution; (b) cross-section of the 128th row of the right hand image.

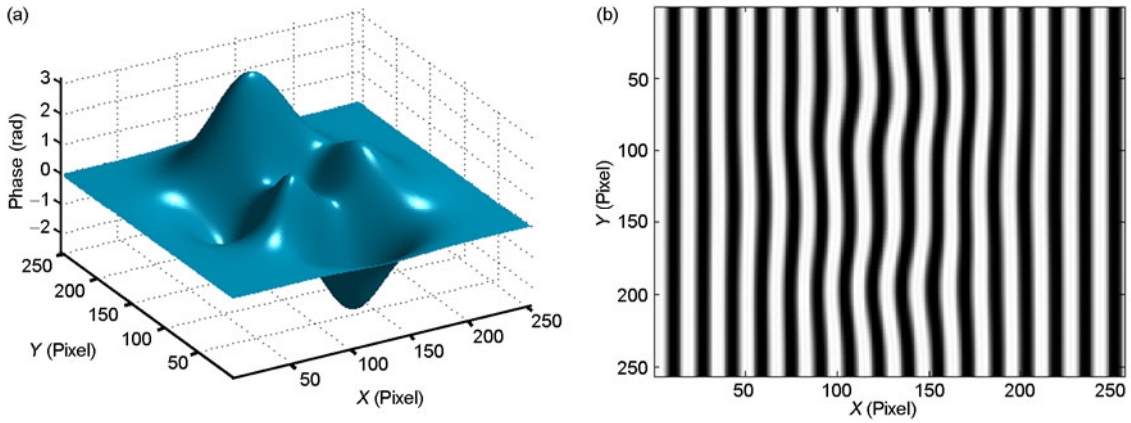

Figure 3 (Color online) The phase distribution of the simulation object (a) and the deformed fringe image of the object (b).

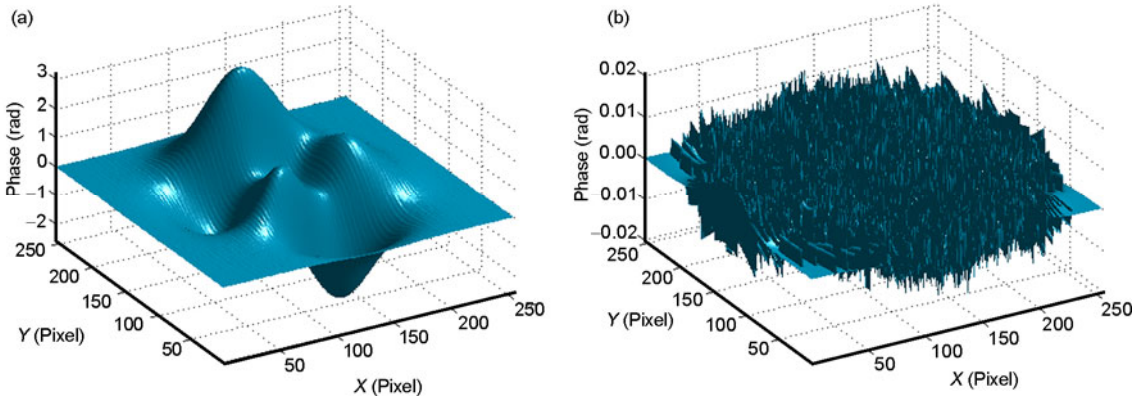

Figure 4 (Color online) Phase distribution using the 5-step phase-shift algorithm (a) and phase relative error distribution (b) .

fluctuation errors in the actual phase and the surface is not smooth. The relative phase error distribution is shown in Figure 4(b).

As shown by the theoretical analysis in Section 2, we use the EMD method to reduce the phase fluctuation error. Figure 5(a) shows the phase distribution of the 128th row of Figure 4(a). By applying the EMD method to Figure 5(a), the phase is decomposed into five IMFs and a residue. Figure 5(b) displays the five IMFs and the residue. We then subtract the high frequency components after decomposition, thus removing the phase fluctuation error (see Figure 5(c)). Figure 5(d) shows the phase distribution obtained using EMD and the Wavelet method. We see that the phase distribution is much smoother using EMD and the Wavelet method. The RMS of the phase profile is approximately 3.152 rad using the EMD and approximately 3.156 rad using the Wavelet method. It is obvious that the proposed method provides a more accurate result. Similarly, the procedure is used for each row of the phase signal of Figure 4(a), and we obtain the desired phase distribution. Figure 6(a) shows the desired phase. The relative phase error is shown in Figure 6(b). Comparing Figures 4(a) and 6(a), we clearly observe that the proposed method can reduce the fluctuation errors and provide a smoother and more accurate result.

To further demonstrate the method reported here, we measure an actual object. We built the 3D shape measurement system using a projector (BenQ MP512) and a camera (DH-HV1351UC). The projector projects five phase-shifted fringe images. The camera captures the reference and deformed fringe images. The size of the image is reduced to 751×631 pixels. Figure 7(a) and (b) show one of the five reference fringe images and the deformed fringe image of the object (complex face model). Figure 7(c) and (d) show the 3D measurement results before and after phase error reduction. The RMS of the phase profile is approximately 4.762 rad. The results show that the surface of the phase before error reduction is very rough and becomes smooth once the EMD method is applied.

In addition, we measured a heart model using the other measuring equipment. The projector is SANYO PRO xtrax and the CCD camera is MVC-II-1M .The size of the image is reduced to 241×241 pixels. Figure 8(a) and (b) show one of the five reference fringe images and the deformed fringe image for the object (heart model). Figure 8(c) and (d) show the 3D measurements before and after phase error reduction.

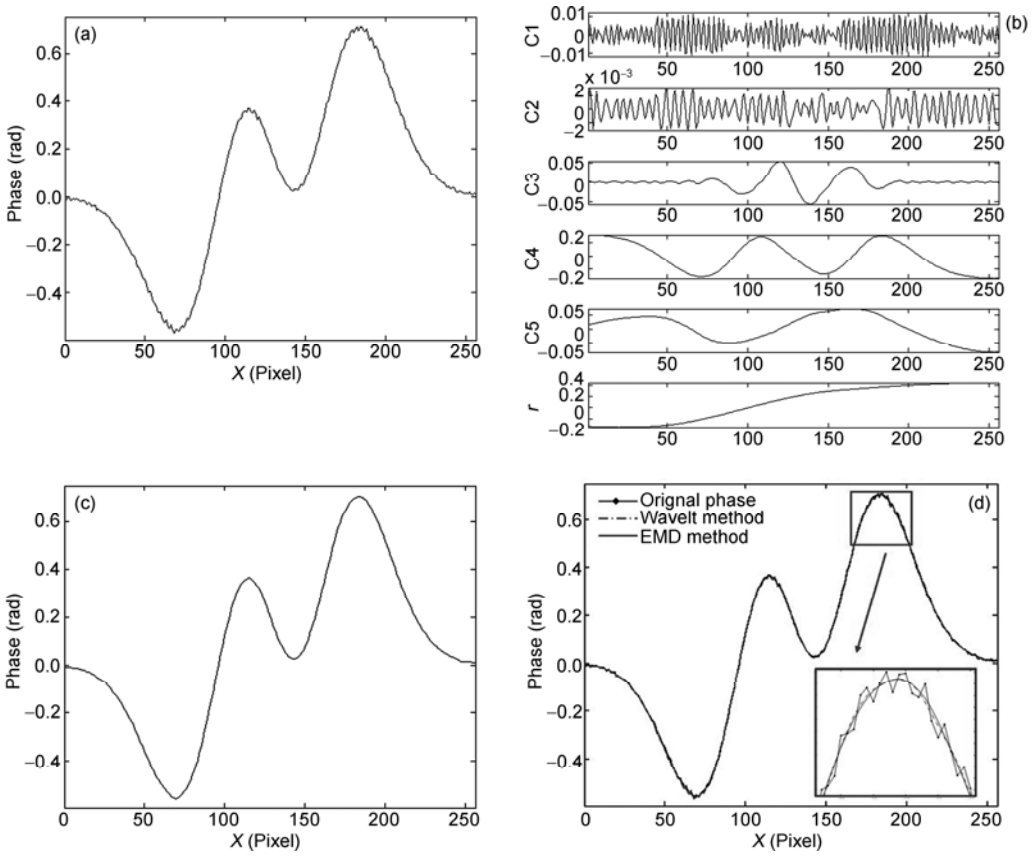

Figure 5 Phase error reduction. (a) Cross-section of the 128th row of Figure 4(a); (b) the decomposition result using EMD; (c) phase distribution after phase error reduction using EMD; (d) comparison of the phase distribution obtained using EMD and the wavelet method.

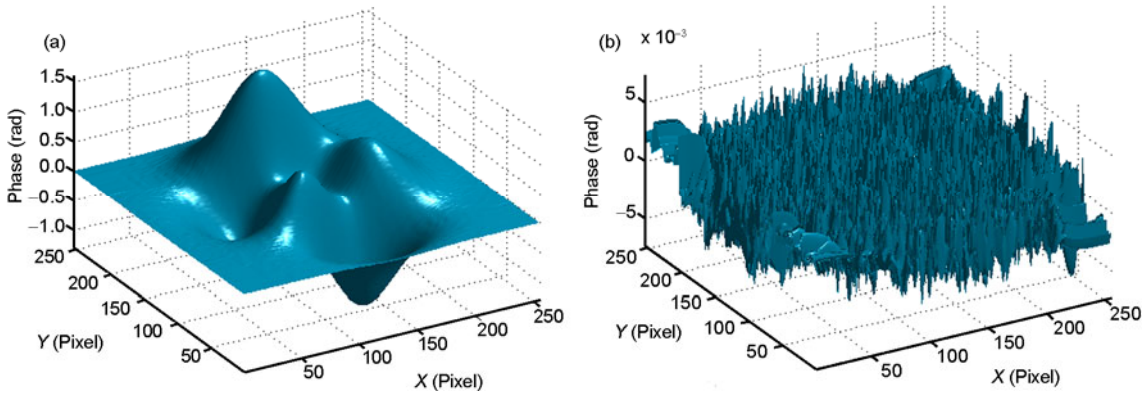

Figure 6 (Color online) Phase distribution after phase error reduction with the algorithm proposed in this paper (a) and (b) phase relative error distribution.

The RMS of the phase profile is approximately 4.263 rad. The reconstructed 3D surface after phase reduction is much smoother. These computer simulation and experimental results confirm the phase error reduction method significantly improved the measurement accuracy.

3 Conclusions

This study introduced the empirical mode decomposition (EMD) method into Phase Measurement Profilometry (PMP) for reducing the phase error. We showed that the phase error was caused by the nonlinear response of the measurement system. The influence of the nonlinear error of the measurement system was considerable in the calculated phase using the conventional five-step phase-shifting method. To reduce this influence, we performed a theoretical analysis, finding that the phase error can be eliminated by the EMD method. Computer simulation and experiments were conducted to show the feasibility of our method.

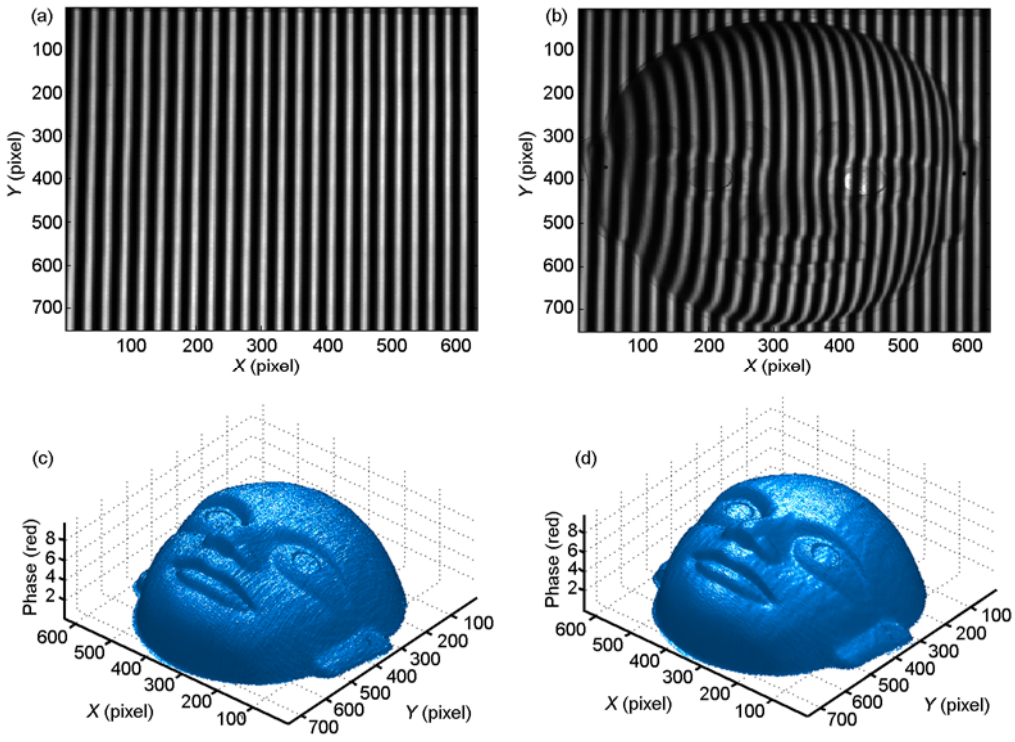

Figure 7 (Color online) A reference fringe image(a); a deformed fringe image (b); phase distribution before error reduction (c) and (d) phase distribution after error reduction.

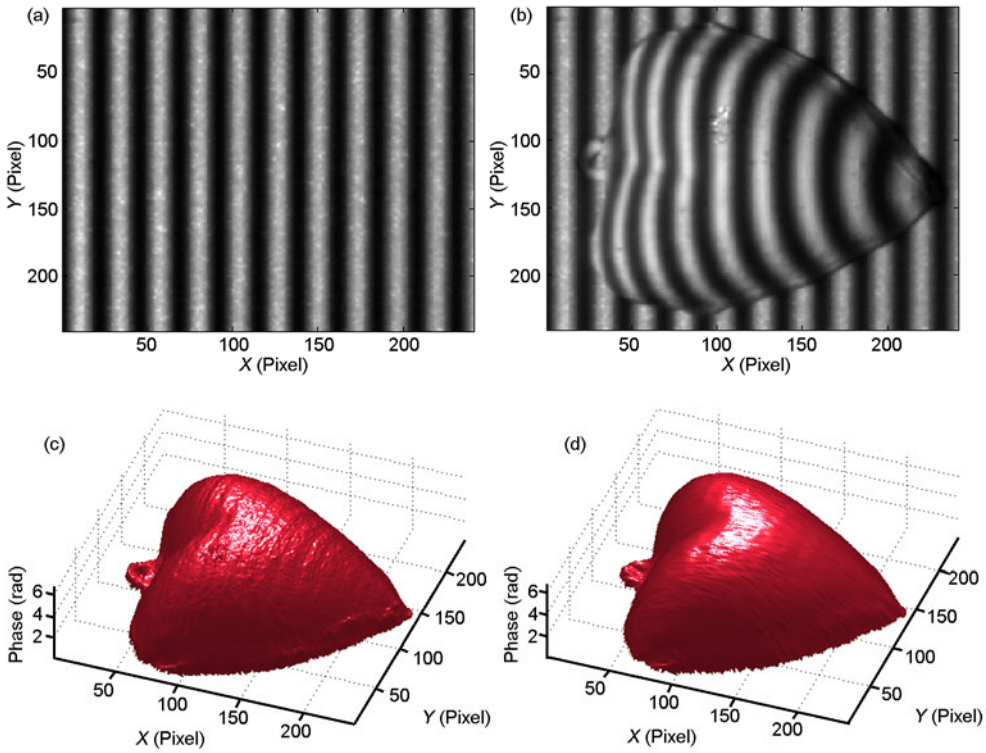

Figure 8 (Color online) The reference fringe image (a); a deformed fringe image (b); phase distribution before error reduction (c) and (d) phase distribution after error reduction.

This work was sipported by the National Natural Science Foundation of China (*61128012, 60978043, 61061160503*), *and the Research Grants Council of the Hong Kong Special Administrative Region* (*9041577*).

1 Zhang S, Weide D V D, Oliver J. Superfast phase-shifting method for 3-D shape measurement. Opt Express, 2010, 18: 9684–9689
2 Notni G H, Notni G. Digital fringe projection in 3D shape measurement: An error analysis. Proc SPIE, 2003, 5144: 372–380
3 Cai C L, Li X H, Wu H T, et al. A satellite clock error correction method in the wide area differential system. Chin Sci Bull, 2009, 54: 4616–4623
4 Lu C X, Tan Y H, Zhu B C, et al. Improved innovation-based adaptive Kalman filter for dual-frequency navigation using carrier phase. Sci China Inf Sci, 2010, 53: 2653–2663
5 Xia N, Han D, Zhang G F, et al. Study on attitude determination based on discrete particle swarm optimization. Sci China Tech Sci, 2010, 53: 3397–3403
6 Creath K. Error sources in phase-measuring interferometry. Proc SPIE, 1992, 1720: 428–435
7 Zhang S, Yau S. Generic non-sinusoidal phase error correction for three-dimensional shape measurement using a digital video projector. Appl Opt, 2007, 46: 36–43
8 Pan B, Qian K, Huang L, et al. Phase error analysis and compensation for non-sinusoidal waveforms in phase-shifting digital fringe projection profilometry. Opt Lett, 2009, 34: 416–418
9 Xiong L, Jia S. Phase-error analysis and elimination for non-sinusoidal waveforms in Hilbert transform digital-fringe projection profilometry. Opt Lett, 2009, 34: 2363–2365
10 Huang N E, Shen Z. The empirical mode decomposition and the Hilbert spectrum for nonlinear and non-stationary time series analysis. Proc R Soc Lond Ser A, 1998, 454: 903–995
11 Wu F, Qu L. An improved method for restraining the end effect in empirical mode decomposition and its applications to the fault diagnosis of large rotating machinery. J Sound Vib, 2008, 314: 586–602
12 Su H J, Li J L, Su X Y. Phase algorithm without the influence of carrier frequency. Opt Eng, 1997, 36: 1799–1805